Experimental study on ammonia/hydrogen/air combustion in spark ignition engine conditions

Charles Lhuillier, Pierre Brequigny, Francesco Contino, Christine Mounaïm-Rousselle

Experimental study on ammonia/hydrogen/air combustion in spark ignition engine conditions

Charles LHUILLIER[a, b, c,1], Pierre BREQUIGNY[a], Francesco CONTINO[b, c], Christine MOUNAÏM-ROUSSELLE[a]

[a] *Laboratoire PRISME, Université d'Orléans, France*

[b] *Thermo and fluid dynamics (FLOW), Vrije Universiteit Brussel, Belgium*

[c] *Combustion and Robust Optimization Joint Research Group, VUB – ULB, Belgium*

Abstract

The mitigation of climate change implies the increasing use of variable renewable energy sources. Energy storage and transport solutions will contribute to ensure the stability, reliability and flexibility of the energy systems in that context. Ammonia is a well-known chemical of formula NH_3 and, amongst other electrofuels, a promising energy carrier and carbon-free combustible fuel. In the present experimental study, engine performance, combustion characteristics and pollutant emissions of a recent spark ignition engine fueled with premixed ammonia/hydrogen/air mixtures were assessed. Gaseous ammonia blends in a wide range of hydrogen fuel fractions and equivalence ratios were tested at two different engine loads. Results show performances comparable with conventional fuel operation when the appropriate promotion strategies are used. Specifically, blending up to 20% hydrogen in the fuel by volume improves the cyclic stability and avoids misfires, while granting the best work output and indicated efficiencies near stoichiometry. Higher hydrogen fractions result in depleted efficiency, attributed to higher wall heat losses. The combustion duration is directly correlated to the LBV of the mixtures, thus being accelerated by hydrogen blending. The accelerating effect of hydrogen is particularly remarkable during the initial stage of the combustion. Hydrogen appears therefore mainly as an ignition promoter. Increasing the engine load improves the furnished work and allows to extend the operating boundaries in terms of mixture composition.

Keywords

Ammonia ; Hydrogen ; Spark ignition engine ; Sustainable fuel ; Performance ; Emissions

[1] Corresponding author. Address: Laboratoire PRISME, Université d'Orléans, 8 rue Léonard de Vinci, 45072 Orléans, France. E-mail : charles.lhuillier@ univ-orleans.fr

1. Introduction

Ammonia (NH_3) is increasingly considered as a prominent enabler of the ongoing transition towards high shares of Variable Renewable Energy Sources (VRES) in the energy systems, as stated in *The Future of Hydrogen*, a recent report by the International Energy Agency [1]. Indeed, VRES should account for more than 50% of the total primary energy supply by 2050 to comply with the global warming mitigation objectives of the Paris Agreement, according to the Intergovernmental Panel on Climate Change [2]. In this new energy paradigm, energy storage and transport solutions will contribute to the efficiency and sustainability of the energy systems.

Ammonia, along with other electrofuels, i.e. energy-dense chemicals producible from electricity, water and any other renewable feedstock, appears as such a renewable and carbon-free energy carrier. Its exhibits a high hydrogen content of 17.8% by mass, a volumetric energy density of 11.3 GJ/m^3 when stored in liquid form at 1.1 MPa and 300 K, and is as such an efficient hydrogen carrier.

In order to avoid costly ammonia-to-hydrogen conversions and depending on the final energy use, direct ammonia combustion can be considered. Related research efforts have been summarized recently by Valera-Medina et al. [3]. Those mainly focus on overcoming the unfavorable combustion properties of NH_3, illustrated in Table 1 by its low Laminar Burning Velocity (LBV), high auto-ignition temperature and narrow flammability range, as well as addressing the challenge of nitrogen-based pollutant emissions. To that aim, several practical combustion technologies were investigated, including gas turbines [4,5], compression-ignition engines, mostly in dual fuel configurations [6-16] and Spark Ignition (SI) engines [17-34].

Table 1. Ammonia properties and comparison with other fuels at 300 K and 0.1 MPa. Data from [3,23,35]

	Ammonia	Methanol	Hydrogen	Methane	Gasoline
Formula	NH_3	CH_3OH	H_2	CH_4	-
Storage	Liquid	Liquid	Compressed	Compressed	Liquid
Storage temperature (K)	300	300	300	300	300
Storage pressure (MPa)	1.1	0.1	70	25	0.1

Density under storage conditions ($kg.m^{-3}$)	600	785	39	187	~740
Lower Heating Value (LHV) ($MJ.kg^{-1}$)	18.8	19.9	120	50	44.5
Volumetric energy density ($GJ.m^{-3}$)	11.3	15.6	4.7	9.35	33
Stoich. air-fuel ratio by mass	6.05	6.44	34.6	17.3	15
LBV @ $\phi = 1$ ($m.s^{-1}$)	0.07	0.36	3.51	0.38	0.58
Auto-ignition temp. (K)	930	712	773-850	859	503
Research Octane Number	130	119	>100	120	90-98
Flammability limits in air (vol.%)	15-28	6.7-36	4.7-75	5-15	0.6-8

The flexibility of the internal combustion engine makes it appealing for NH_3 fuel use, especially when assisting the ignition with a spark. SI engines can be run on ammonia blends at high compression ratio (CR) without risk of engine knock thanks to the high octane number of ammonia. This was demonstrated in early studies, where single-cylinder and multi-cylinder SI engine were successfully run on pure ammonia fuel [17–19]. However, gasoline-like performances were only achieved by using one or several promoting strategies, including an improved ignition system, increasing the engine load or CR and H_2 doping of the NH_3 fuel. A minimum H_2 amount depending on the engine speed and CR of some percent by mass was necessary to ensure satisfying performance and decrease NH_3 emissions but at the cost of increased NOx emissions.

Contemporary studies also investigated ammonia/gasoline fueling of SI engine, either to reduce carbon-based emissions of gasoline engines, or to promote the combustion with ammonia as a main fuel. Granell et al. proposed a 70% NH_3 / 30% gasoline blend by energy as a good trade-off at full load in a Collaborative Fuel Research (CFR) engine [21,22]. The authors suggested supercharging the engine instead of increasing the CR, due to the detrimental thermodynamic consequences of the early spark advance required by the NH_3 fuel. Engine-out NH_3 emissions proportional to the NH_3 input are reported, up to 22000 ppmvw for stoichiometric

NH_3/air at CR=10:1. Ryu et al. investigated direct gaseous NH_3 injection in a CFR engine (CR = 10:1) with gasoline as the base fuel, and reported acceptable performance but high nitrogen-based specific emissions [36]. The same authors suggested to partly dissociate NH_3 prior to direct injection, to use the beneficial effect of H_2 on the combustion efficiency, and reduce the pollutant emissions [32].

That capability of molecular hydrogen of being producible in-situ through ammonia dissociation, possibly by recycling exhaust heat and requiring no additional tank, grants it a potential advantage over other combustion-promoting fuels. Therefore, further researchers investigated the use of hydrogen-enriched ammonia in SI engines. Koike et al. studied a single-cylinder SI engine (CR = 14:1) fueled with premixed stoichiometric NH_3/H_2/air and NH_3/gasoline/air mixtures [29]. Stable operation was achieved for 10 – 60 LHV% of H_2 (12.6 – 66.1 mol.%) or 40 – 100 LHV% gasoline (8 – 100 mol.%) fuel fractions for light load (Indicated Mean Effective Pressure, *IMEP* = 0.2 MPa), and up to 100 % NH_3 for high load (*IMEP* = 0.8 MPa). An auto-thermal cracker was successfully operated to provide H_2 from NH_3 dissociation. Similarly, Frigo and Gentili studied a twin-cylinder commercial SI engine fueled with premixed stoichiometric NH_3/H_2/air mixtures at half and full load and several engine speeds [27]. They found a minimum hydrogen-to-ammonia energy ratio of 7% at full load and 11% at half load to ensure stable engine operation, but with decremented performance with respect to gasoline operation. Maximum NOx emissions of 1700 ppm and surprisingly low NH_3 emissions are reported, although the latter have only been detected through a threshold sensor. Comotti and Frigo extended the previous study by demonstrating the successful use of a catalytic cracking reactor for in-situ H_2 production [24]. Mørch et al. fueled a CFR engine with NH_3/H_2 blends at various CR, with a metal ammine complex as NH_3 reservoir [23]. They showed increased engine performance and similar NOx emissions with respect to gasoline operation, thanks to the possibility of knock-free CR increase. Best performance is found at stoichiometry for 10 mol.% H_2 in the fuel. Selective Catalytic Reduction is suggested as a meaningful way to mitigate NOx emissions, thanks to appropriate exhaust temperatures and NH_3 availability, with the major challenge of avoiding NH_3 slip at the exhaust. Westlye et al. focused on nitrogen-based pollutant emissions of a CFR engine fueled with 80 mol.% NH_3 / 20 mol.% H_2 lean blends, and further demonstrated the feasibility of SCR for pollutants mitigation [30].

Therefore, the suitability of ammonia as an efficient carbon-free SI engine fuel has been demonstrated in the literature, and the relevance of H_2 as a combustion promoter has been underlined. However, most of the experimental data were obtained in outdated or basic engine geometries and covered only a partial range of mixture compositions. The objective of the present work is thus to actualize and extend the experimental database for NH_3/H_2/air combustion in a SI engine, so as to conduct further analysis that should provide useful understanding on ammonia combustion properties. To that end, one cylinder of a recent commercial SI engine was fueled with premixed gaseous NH_3/H_2/air mixtures for a wide range of mixture compositions at and beyond full load. Measurements for part-load operation close to stoichiometry were published elsewhere [33,34]. The experimental set-up and the operating conditions are first introduced. Extensive data derived from in-cylinder pressure and exhaust gas measurements are then presented, analyzed and discussed.

2. Experimental and numerical methods

2.1. Engine setup

The engine used for the experiments is a recent four-cylinder four-stroke SI engine, retrofitted to a single-cylinder by fueling only one cylinder. The engine specifications are shown in Table 2. This engine benefits from improved aerodynamics, thanks to its piston bowl optimized for gasoline direct injection, granting it a tumble ratio of about 2.4 [37].

Table 2. Engine specifications

Model	PSA EP6DT
Stroke	85.8 mm
Bore	77 mm
Connecting rod length	138.5 mm
Displacement volume	399.5 cm^3
Geometric compression ratio	10.5:1
Valves	4
Engine speed	1500 rpm

A constant engine speed of 1500 rpm is imposed to the engine by an electric motor. A Kübler optical encoder monitors the angular position of the main shaft with a 0.1 Crank Angle Degree (CAD) resolution. Type K thermocouples and piezo-resistive pressure transducers are used to monitor the intake and exhaust temperature and pressure, respectively. The temperature of the cooling fluid is set and monitored at 353 K. The flows of the reactive gases, including dried ambient compressed air, bottled ammonia and bottled hydrogen are monitored by means of Brooks thermal mass flowmeters with 0.7% accuracy on their full scale, preheated to the intake temperature of 323 K and premixed in an intake plenum prior to injection. The original spark plug is used with a coil charging time of 2 ms. A water-cooled AVL piezoelectric pressure transducer measures the in-cylinder pressure with a 0.1 CAD resolution and a measuring range of 0 – 25 MPa. The absolute in-cylinder pressure is obtained by equalizing the previous signal with the mean absolute intake pressure, P_{in}, 20 CAD after inlet valve opening (pressure pegging). The exhaust gas composition is monitored by means of a Gasmet Fourier-Transform InfraRed (FTIR) gas analyser. The wet exhaust concentrations of H_2O, NH_3, NO, NO_2 and N_2O were measured simultaneously for each test with a time step of 5 s. Figure 1 shows a scheme of the experimental setup.

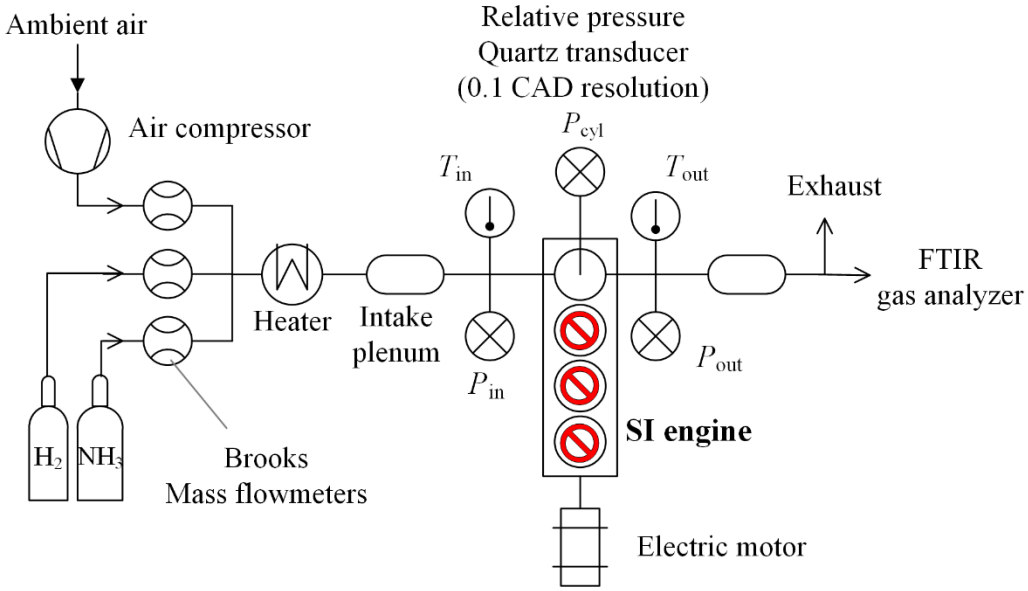

Figure 1. Scheme of the experimental setup

2.2. Operating conditions

The global stoichiometric reaction of NH_3/H_2/air combustion is as:

$$\left(1-x_{H_2}\right)NH_3 + x_{H_2}H_2 + \frac{3-x_{H_2}}{4}(O_2 + 3.76N_2) \rightarrow \left(\frac{3-x_{H_2}}{2}\right)H_2O + \left(\frac{1-x_{H_2}}{2} + 3.76 * \frac{3-x_{H_2}}{4}\right)N_2 \quad (1)$$

with x_{H_2}, the hydrogen molar fraction in the fuel mixture. Non-stoichiometric mixtures are defined by the equivalence ratio, ϕ:

$$\phi = \frac{\frac{X_{H_2} + X_{NH_3}}{X_{air}}}{\left(\frac{X_{H_2} + X_{NH_3}}{X_{air}}\right)_{st}} \quad (2).$$

X_s represents the molar fraction of the species s in the reactive mixture, and subscript "st" stands for stoichiometric. The stoichiometric air/fuel ratio by mass is about 6 for pure NH_3 fuel and thus more than twice smaller than for gasoline, as shown in Table 1, but increases slightly with hydrogen enrichment. The investigated operating conditions are summarized in Table 3, and are intended to cover a broad range of mixture compositions representative of possible ammonia/hydrogen operating modes of SI engines at and beyond full load. In order to make optimal performance considerations, the spark ignition timing (SIT) is set to maximize the net Indicated Mean Effective Pressure ($IMEP_n$), a quantification of the net work furnished by the expanding gas on the piston. This is equivalent to the Maximum Brake Torque (MBT) timing, but the absence of direct torque measurement due to the friction losses caused by the three unproductive pistons led to the previous approach. Cycle-to-cycle variability is considered by recording 100 consecutive pressure cycles for each test. Averaged values over 100 cycles are presented in this paper.

Table 3. Overview of the operating conditions.

Intake temperature (K)	Intake pressure (MPa)	H_2 fraction in the fuel		ϕ
323	0.1, 0.12	By volume	[0 – 0.6]	[0.6 – 1.2]
		By energy (LHV)	[0 – 0.54]	
		By mass	[0 – 0.15]	

2.3. Combustion analysis and laminar burning velocity calculation

A precise determination of the CR and detection of the Top Dead Center (TDC) position is required for an accurate analysis based on the in-cylinder pressure signal and calculated in-cylinder volume. Therefore, the methodology proposed by Tazerout et al. [25-26] for CR determination and pressure-volume lag elimination is implemented within the classical analysis of the cylinder pressure-volume data proposed by Heywood [40]. Crevices effects are neglected and no in-cylinder mass variation are considered between Inlet Valve Closing (IVC) and Exhaust Valve Opening (EVO). Performance indicators such as the $IMEP_n$ and its coefficient of variation over 100 cycles COV_{IMEP} can be deduced accurately, as well as the bulk in-cylinder temperature between IVC and EVO. The latter is determined by means of the ideal gas law, assuming the gas temperature to be equal to the inlet temperature T_{in} = 323 K at IVC. The combustion analysis is also performed by calculating the net heat release rate (HRR) by means of the first law of thermodynamics in a one-zone model. The in-cylinder heat capacity at constant pressure is calculated using the bulk in-cylinder temperature and an in-cylinder charge composition modeled by a representative mixture of burned and unburned gases weighted by the burned mass fraction (that can be determined iteratively), assuming complete combustion. The gross HRR from the combustion is estimated by considering the wall heat losses by means of the model of Hohenberg [41]. Combustion phasing in the cycle is established by assessing the crank angles at which 10%, 50% and 90% of the cumulated gross heat release is reached, yielding CA10, CA50 and CA90, respectively.

The laminar burning velocity of the reactive mixtures under the thermodynamic conditions at SI timing is calculated by means of a newly developed LBV correlation for NH_3/H_2/air flames proposed by Goldmann and Dinkelacker [42] on the basis of the detailed reaction mechanism of Mathieu and Petersen [43]. This correlation takes the presence of hydrogen in the fuel into account and was validated against measurements at normal temperature and up to 500 kPa of pressure for various mixture compositions.

3. Results and discussion

3.1. Engine performance

The engine was operated successfully with an excellent cycle-to-cycle stability for a wide range of H_2 fractions and equivalence ratios, when the spark ignition was sufficiently advanced, as shown in Figure 2a and 2b. An acceptable cyclic variability boundary was set at $COV_{IMEP} \leq 5\%$ (coefficient of variation of the $IMEP_n$), but most of the conditions verified $COV_{IMEP} \leq 3\%$, as shown in Figure 2c and 2d. It should be emphasized here

that stable operation could be achieved for a stoichiometric NH_3/air mixture for both intake pressures. Only mixtures with high hydrogen fraction were found suitable for very lean operation. When increasing the NH_3 content in the fuel, advancing the SI timing is unsurprisingly required to maintain the cyclic stability and reach the maximum power output, as shown in Fig. 2a and 2b. This is primarily attributed to the low LBV of NH_3 that slows down the early stages of the flame propagation, and explains the bell-shaped dependence of the SI timing to the equivalence ratio. For a given fuel blend, the SI timing closest to TDC is obtained near stoichiometry, corresponding to the region of maximum LBV.

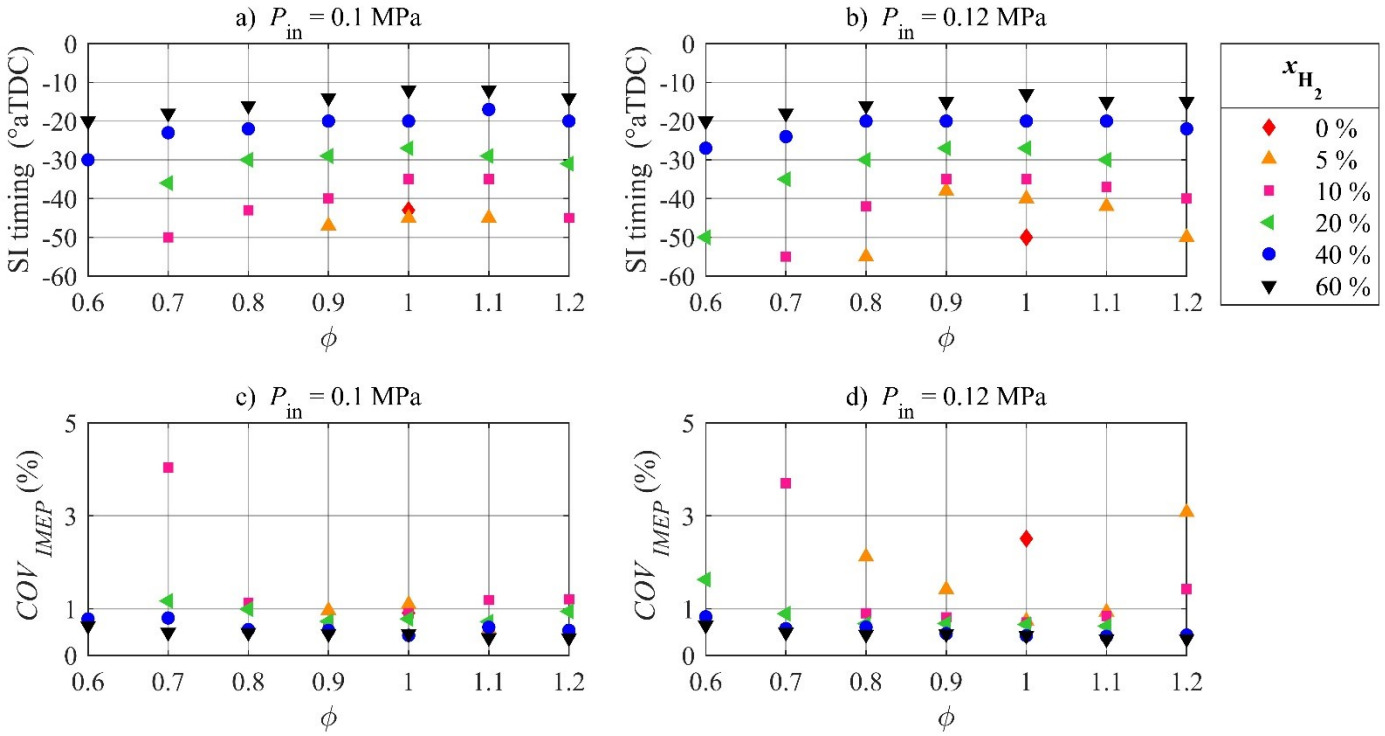

Figure 2. Optimized Spark Ignition Timing and Coefficient of Variation of the $IMEP_n$.

Figure 3 shows the $IMEP_n$ as a quantification of the piston work, along with a "Fuel Mean Effective Pressure" (*FuelMEP*) for the ratio between the cyclic energy input on a LHV basis and the displaced volume. The *FuelMEP* is an increasing function of the intake pressure and the equivalence ratio, but volumetric hydrogen enrichment of the fuel at given ϕ does not modify the energy content of the fuel/air mixture, as the lower volumetric energy density of H_2 happens to be compensated by its lower stoichiometric air-fuel ratio, as shown in Fig. 3c and 3d. As a result, the $IMEP_n$ increases as the equivalence ratio is increased up to 1.1, as shown in Fig. 3a and b. In spite of excess fuel presence when ϕ = 1.1, the extra work obtained at this equivalence ratio may be explained by the maximum LBV reached close to that value as compared to stoichiometry [42], allowing to operate closer to an ideal thermodynamic cycle. Further increase of the equivalence ratio only results

in more excess fuel with no LBV benefit, thus explaining the stagnation or decrease of the $IMEP_n$ when ϕ = 1.2. In spite of nearly identical *Fuel MEP*, mixtures with low to moderate hydrogen fractions exhibit higher maximum $IMEP_n$ than highly enriched mixtures, consistently with the observations in [23] . Unsurprisingly, increasing the intake pressure allows to increase the power output up to values typical of full-load conventional fuel operation of the engine.

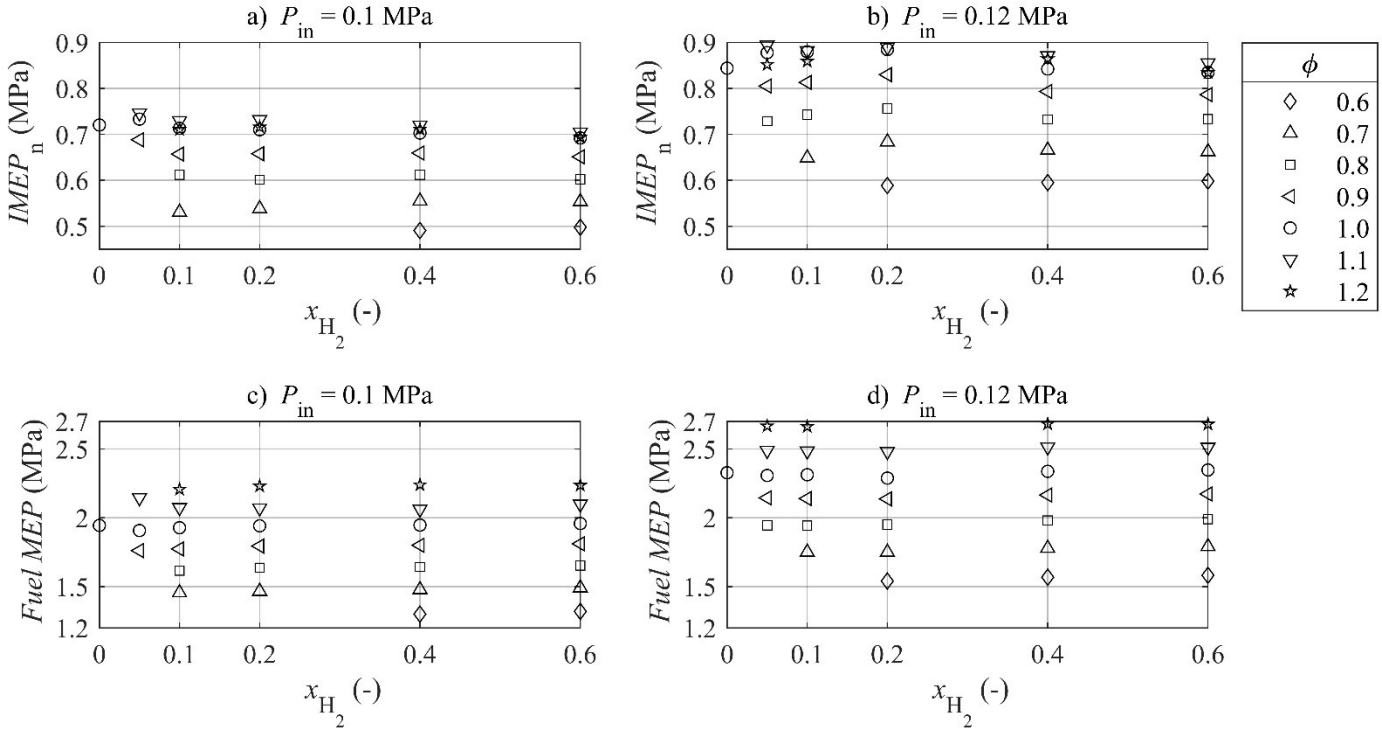

Figure 3. Net Indicated Mean Effective Pressure and Fuel Mean Effective Pressure.

The ratio of the $IMEP_n$ and the *Fuel MEP* yields the indicated efficiency and is shown in Figure 4. It is optimal for slightly hydrogen-enriched near-stoichiometric lean mixtures with highest values close to 39%. The dependence on the intake pressure is not fully consistent but tends to indicate a slight improvement of the indicated efficiency as the load is increased. Highly hydrogen-enriched near-stoichiometric mixtures experience a depleted indicated efficiency, assumedly due to higher wall heat losses linked to high flame temperatures, but the efficiency improves when operating towards leaner equivalence ratios while the flame temperatures decrease accordingly.

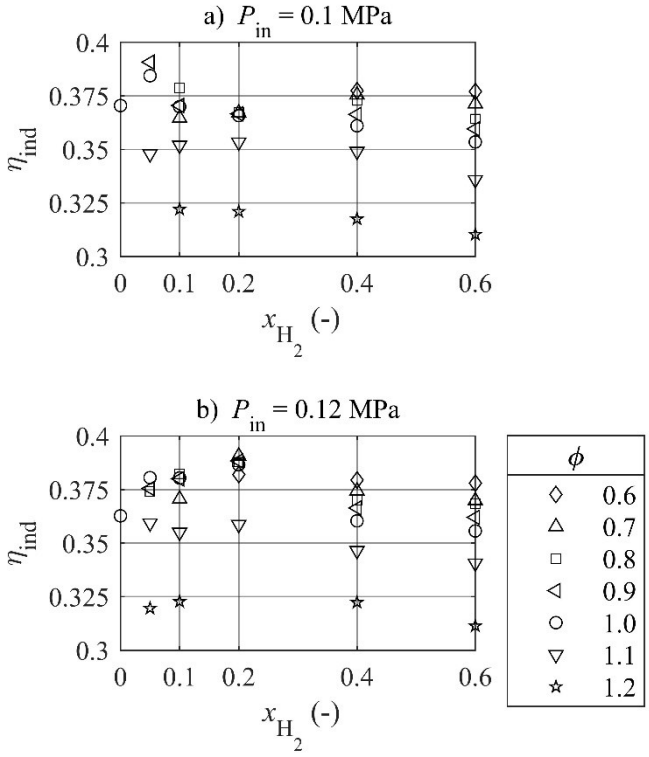

Figure 4. Indicated efficiency.

3.2. Combustion analysis

Figure 5 shows the in-cylinder pressure data, along with the bulk in-cylinder temperature for stoichiometric mixtures. Pentagram symbols identify the spark ignition. While the thermodynamic conditions at ignition may differ with respect to the fuel hydrogen fraction due to the optimization of the SIT, the magnitude of the in-cylinder pressure rise remains comparable especially for atmospheric intake pressure. However, the estimated bulk in-cylinder temperatures shown in Figs. 5c and 5d exhibits higher peaks for highly hydrogen-containing mixtures, thus supporting the assumption of higher wall heat losses for such mixtures near stoichiometry.

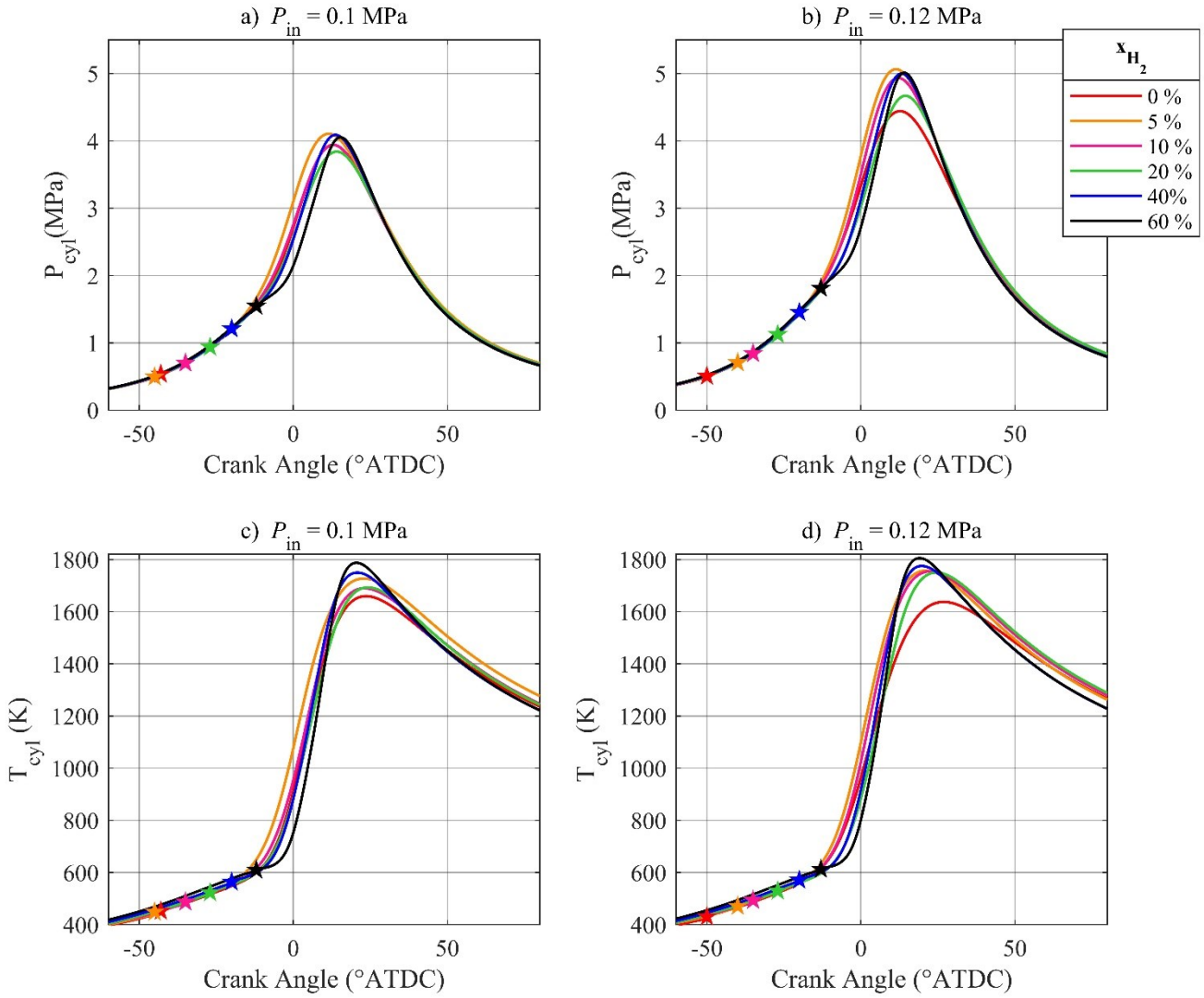

Figure 5. Measured in-cylinder pressure and estimated bulk in-cylinder temperature for ϕ = 1.1. Symbols: spark ignition.

Remarkably, the crank angle of occurrence of the maximum in-cylinder pressure is weakly affected by the variations of the mixture composition, as shown in Figure 6. This indicates that, in spite of a wide variation range of the spark ignition timing, the peak in-cylinder pressure is almost constantly phased in the cycle when the optimum $IMEP_n$ is reached. However, a certain data scatter remains, probably partly due to the manual tuning of the optimized spark ignition timing.

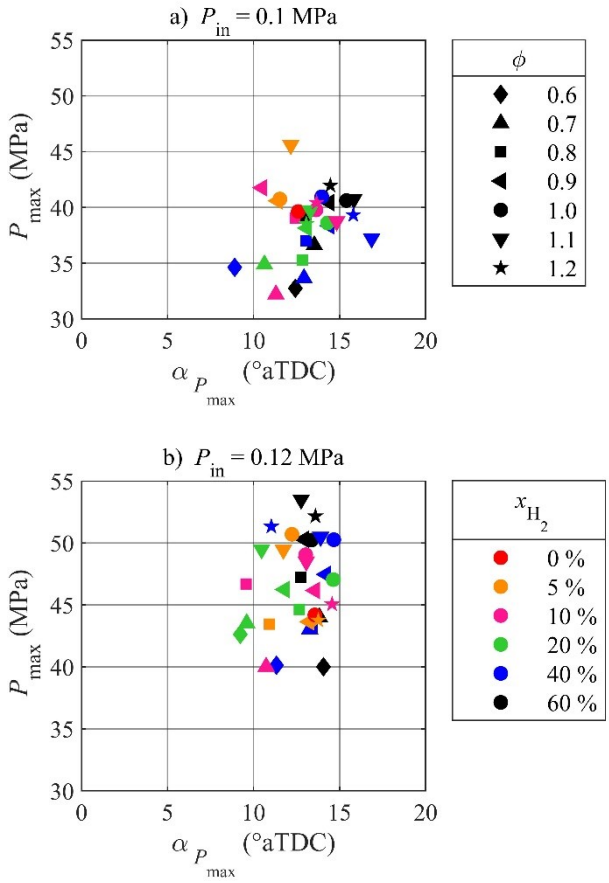

Figure 6. Maximum in-cylinder pressure as a function of its crank angle of occurrence, $\alpha_{P_{max}}$.

Even though no other major differences are observed on the in-cylinder pressure and temperature curves for different mixtures, the composition of the mixtures does impact the heat release rate and hence the duration of the combustion phases. This is highlighted in Figure 7, where the flame initiation phase between SIT and CA10, the first flame propagation phase between CA10 and CA50 and the combustion duration between CA10 and CA90 are shown as a function of the equivalence ratio in the case P_{in} = 0.12 MPa. Similar results are obtained at P_{in} = 0.1 MPa and are thus not presented here. For hydrogen fuel fractions lower than 20%, the duration of the combustion phases decreases at a faster rate than the hydrogen fraction is increased. It then becomes nearly proportional to the hydrogen fuel fraction for 40% and 60% H_2. The effect of hydrogen on the initiation phase is always greater than proportional, with 34% and 62% acceleration relative to the pure NH_3 case for stoichiometric mixtures with 10% and 40% H_2, respectively. This may be partly due to the more favorable thermodynamic conditions due to an ignition closer to TDC in the latter cases, but also to the increase of the turbulent flame speed due to hydrogen addition. The influence of the equivalence ratio appears mainly correlated to the LBV of the mixture, since the different phases are accelerated when increasing ϕ from lean to stoichiometric and decelerated when further increasing it from stoichiometric to rich. A stagnation

or further acceleration of the phases as a function of ϕ is observed for mixtures with high H_2 content, due to the shift of the peak LBV towards richer mixtures in those cases. This is highlighted in Figure 8, where the different combustion phases are plotted as a function of the LBV, estimated at the thermodynamic conditions at SIT (cf. Section 2.3).

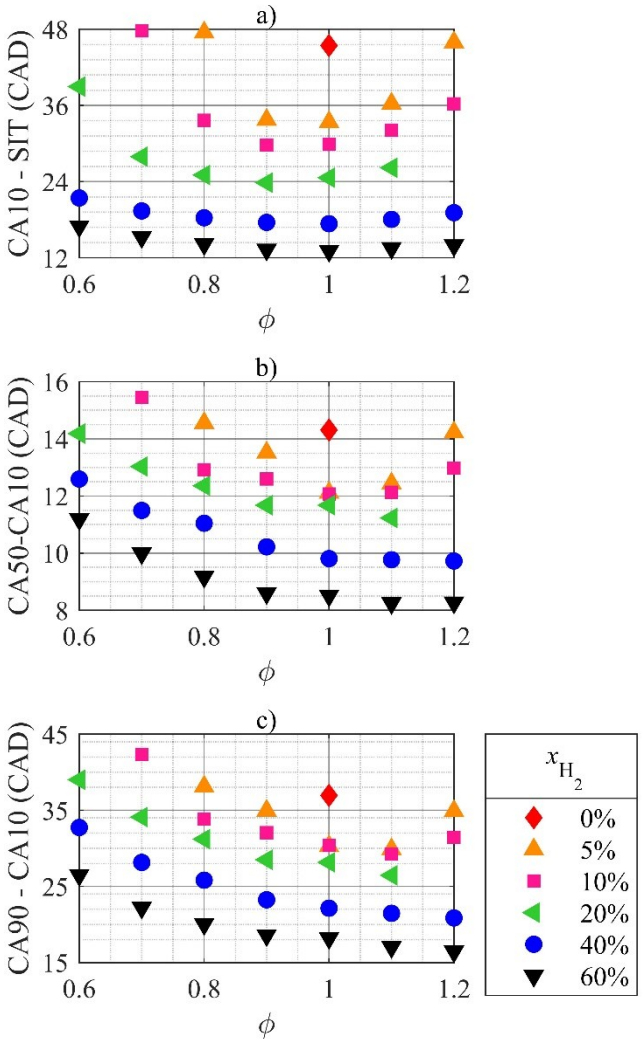

Figure 7. Combustion phases at P_{in} = 0.12 MPa. a) Initiation phase. b) Propagation phase. c) Combustion duration.

A clear non-linear correlation between the duration of the different combustion phases and the LBV of the mixture at SIT is observed, that seem to be independent of the hydrogen fraction in the case of the propagation phase and the bulk combustion duration. The data are more scattered for the initiation phase, probably due to different ignition behavior, as well as to the manual tuning of the SI timing. The effects of hydrogen are believed to be critical during that phase, since it has a strong influence on the flame response to stretch and thermal-diffusive instabilities, and thus on the turbulent flame speed that could explain the different

slopes in Fig. 8a. Once a quasi-steady combustion regime has been reached, around CA10, the maximal flame stretch may be reached, thus explaining the dependence of the combustion duration on the LBV only.

The following empirical expression of the correlation between the combustion duration and s_L^0 at P_{in} = 0.12 MPa was determined by means of a least-square algorithm:

$$CA90 - CA10 = 20.0037 \cdot \exp(-11.7506 \cdot s_L^0) + 27.9146 \cdot \exp(-0.5374 \cdot s_L^0) \quad (3).$$

It appears important to notice that H_2-containing mixtures with lower LBVs than stoichiometric pure NH_3 were successfully operated in the engine, thus indicating that the LBV is not the only governing parameter of NH_3 combustion in the engine.

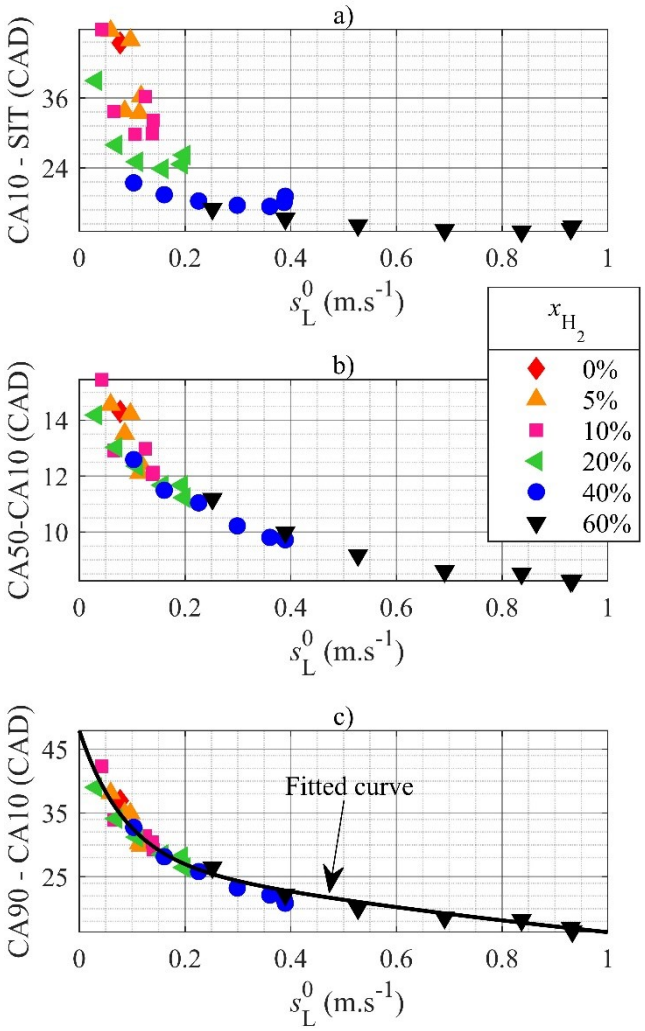

Figure 8. Combustion phasing at P_{in} = 0.12 MPa as a function of the calculated mixture LBV under SIT thermodynamic conditions.

3.3. Pollutant emissions

In order to wrap-up this analysis, pollutant exhaust emissions are shown in Figure 9. Only the measurements for an intake pressure of P_{in} = 0.12 MPa are depicted, since no qualitative difference with the other case was observed. NH_3 emissions increase monotonically with the NH_3 fraction in the fuel, as shown in Fig. 9a. Minimal emissions are observed for near-stoichiometric lean conditions, tending towards leaner mixtures as H_2 is added. That observation is not unexpected since it is the usual region for maximum combustion efficiency, combining the absence of excess fuel with the best reactivity properties. Increasing the hydrogen content allows to extend the range of acceptable reactivity towards leaner mixtures. When the equivalence ratio is increased above stoichiometry, the emissions increase significantly due to the presence of excess fuel and incomplete combustion, reaching very high values of more than 15,000 ppmv. Heading towards very lean mixtures, the NH_3 emissions increase as well, because of poor combustion efficiency.

NOx emissions are shown in Fig. 9b. Minimal values are obtained for rich mixtures with high ammonia content. Mixtures with high H_2 fuel fractions exhibit the highest emissions, probably due to higher flame temperatures that promote thermal NOx formation. Maximal values are found for equivalence ratio 0.8-0.9, as could be expected due to the presence of excess oxygen. Very high values up to 9000 ppm are observed at lean conditions, while low values well below 500 ppm are seen at rich conditions, possibly after partial recombination with unburned NH_3 in the exhaust pipe.

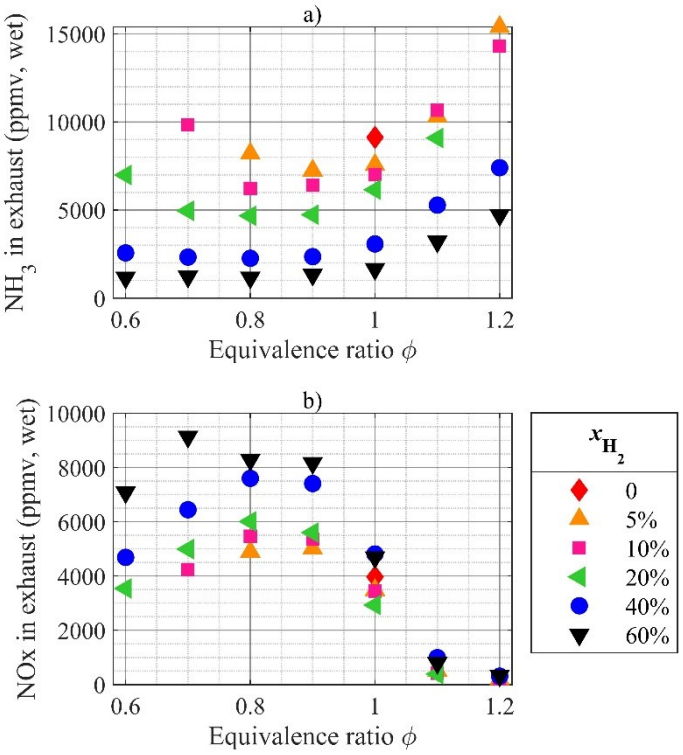

281

282 **Figure 9.** Pollutant emissions in exhaust at P_{in} = 120 kPa. a) Unburned NH_3. b) Total NOx.

283 Either way, mitigation strategies for both NH_3 and NOx are required in order to make ammonia acceptable as
284 a fuel for commercial applications. These could be achieved by means of a SCR catalyst, since both heat and
285 NH_3 reducing agent are available in the exhaust, as demonstrated by Westlye et al. [30]. The feasibility of that
286 approach is verified in Figure 10 that shows the exhaust temperatures measured in the present study. The best
287 operating temperature for usual catalysts are in the range 550-750 K. This could be achieved by operating the
288 present engine in lean conditions. For instance, a mixture with 20% H_2 in the fuel and $\phi = 0.7$ exhibits exhaust
289 temperatures in the appropriate range and also balanced NH_3 and NOx emissions, i.e. NH_3/NOx ≈ 1. Alterna-
290 tively, exhaust gas recirculation could be used to reduce the exhaust temperatures, while taking advantage of
291 the exhaust H_2 concentrations that were evidenced in [33,34] for rich mixtures to promote the combustion. If
292 intake H_2 is to be produced in-situ from ammonia dissociation, the nitrogen co-product will also act as a diluent
293 and thus help reducing the temperatures.

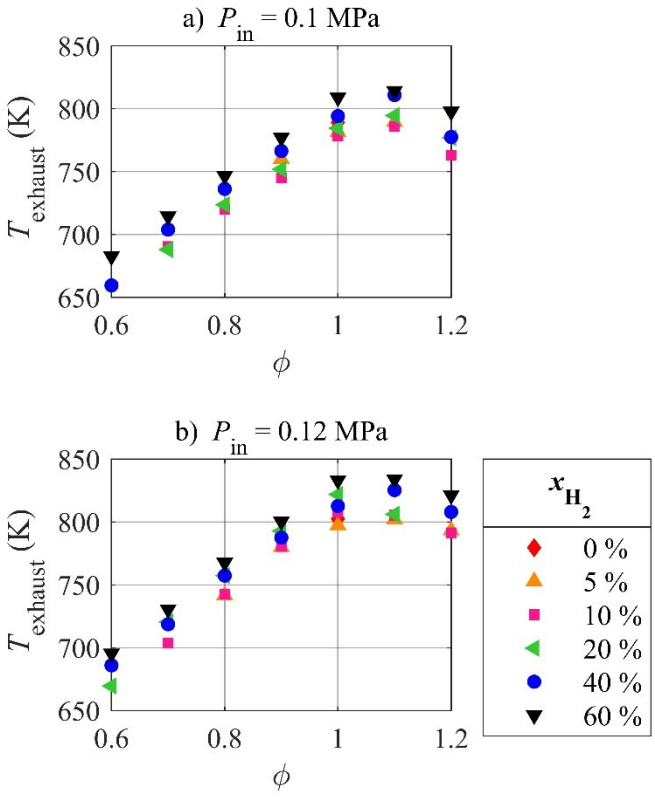

Figure 10. Measured exhaust gas temperature.

4. Summary and conclusions

Experiments were conducted in a modern SI engine in order to assess the feasibility and the characteristics of ammonia combustion at various blended hydrogen fractions, equivalence ratios and intake pressures. In future applications, hydrogen could be provided by in-situ NH_3 dissociation in a catalytic reformer. The main conclusions are as follow:

- A new measurement database of performance, combustion characteristics and emissions data is provided for numerical validation purposes.
- NH_3 is confirmed as a very suitable SI engine fuel for modern engines since neat ammonia operation could be achieved under supercharged conditions, even slight ones.
- Highest indicated pressure and efficiency were achieved at low and moderate hydrogen addition, at slightly fuel-rich and slightly fuel-lean conditions respectively. However, lean mixtures with high hydrogen content also showed promising performance.
- Supercharged operation is expected to be beneficial in all cases, while increasing the compression ratio remains an open question. In that matter, the interest of engine design modification for optimal NH_3 fuel operation still needs to be assessed**.**

- Hydrogen is an ignition promoter, allowing significant performance and stability improvement when added in small quantities, mainly beneficial for the early stages of the combustion. Wall heat losses are thought to play a significant role at high hydrogen fractions.
- The phasing of the combustion is correlated with the Laminar Burning Velocity of the mixture under spark ignition timing conditions, in a non-linear fashion and mainly independently of the hydrogen fraction. However, the LBV does not fully explain the ignition and stability behavior of hydrogen-enriched mixtures with very low LBVs.
- High NOx and NH_3 emissions need to be appropriately mitigated in future applications, possibly by means of already existing technologies. A fuel blend with 20% H_2 and $\phi = 0.7$ exhibited both exhaust temperatures in the range 550-750 K and a NH_3/NOx ratio close to unity, compatible with the use of a dedicated SCR after-treatment system.

Acknowledgements

Funding: This work was supported by the French Government's "Investissement d'Avenir" program: "Laboratoire d'Excellence CAPRYSSES" (Grant No ANR-11- LABX-0006-01).

Declarations of interest

None.

References

[1] International Energy Agency. The Future of Hydrogen. 2019.

[2] Rogelj J, Shindell D, Jiang K, Fifita S, Forster P, Ginzburg V, et al. Mitigation pathways compatible with 1.5°C in the context of sustainable development. 2018.

[3] Valera-Medina A, Xiao H, Owen-Jones M, David WIF, Bowen PJ. Ammonia for power. Prog Energy Combust Sci 2018;69:63–102. doi:10.1016/j.pecs.2018.07.001.

[4] Kobayashi H, Hayakawa A, Somarathne KDKA, Okafor EC. Science and technology of ammonia combustion. Proc Combust Inst 2019;37:109–33. doi:10.1016/j.proci.2018.09.029.

[5] Valera-Medina A, Gutesa M, Xiao H, Pugh D, Giles A, Goktepe B, et al. Premixed ammonia/hydrogen swirl combustion under rich fuel conditions for gas turbines operation. Int J Hydrogen Energy 2019. doi:10.1016/j.ijhydene.2019.02.041.

[6] Pearsall TJ, Garabedian CG. Combustion of Anhydrous Ammonia in Diesel Engines. SAE Tech Pap

1967;670947. doi:10.4271/670947.

[7] Bro K, Pedersen PS. Alternative diesel engine fuels: an experimental investigation of methanol, ethanol, methane and ammonia in a DI diesel engine with pilot injection. SAE Tech Pap 1977. doi:10.4271/770794.

[8] Reiter AJ, Kong SC. Demonstration of compression-ignition engine combustion using ammonia in reducing greenhouse gas emissions. Energy and Fuels 2008;22:2963–71. doi:10.1021/ef800140f.

[9] Reiter AJ, Kong SC. Combustion and emissions characteristics of compression-ignition engine using dual ammonia-diesel fuel. Fuel 2011;90:87–97. doi:10.1016/j.fuel.2010.07.055.

[10] Gill SS, Chatha GS, Tsolakis A, Golunski SE, York APE. Assessing the effects of partially decarbonising a diesel engine by co-fuelling with dissociated ammonia. Int J Hydrogen Energy 2012;37:6074–83. doi:10.1016/j.ijhydene.2011.12.137.

[11] Boretti AA. Novel heavy duty engine concept for operation dual fuel H 2-NH3. Int J Hydrogen Energy 2012;37:7869–76. doi:10.1016/j.ijhydene.2012.01.091.

[12] Gross CW, Kong SC. Performance characteristics of a compression-ignition engine using direct-injection ammonia-DME mixtures. Fuel 2013;103:1069–79. doi:10.1016/j.fuel.2012.08.026.

[13] Ryu K, Zacharakis-Jutz GE, Kong S-C. Performance characteristics of compression-ignition engine using high concentration of ammonia mixed with dimethyl ether. Appl Energy 2014;113:488–99. doi:10.1016/j.apenergy.2013.07.065.

[14] Tay KL, Yang W, Chou SK, Zhou D, Li J, Yu W, et al. Effects of Injection Timing and Pilot Fuel on the Combustion of a Kerosene-diesel/Ammonia Dual Fuel Engine: A Numerical Study. Energy Procedia, vol. 105, 2017, p. 4621–6. doi:10.1016/j.egypro.2017.03.1002.

[15] Pochet M, Truedsson I, Foucher F, Jeanmart H, Contino F. Ammonia-Hydrogen blends in Homogeneous-Charge Compression-Ignition Engine. SAE Tech Pap 2017;2017-24–00. doi:10.4271/2017-24-0087.

[16] Boretti A. Novel dual fuel diesel-ammonia combustion system in advanced TDI engines. Int J Hydrogen Energy 2017;42:7071–6. doi:10.1016/j.ijhydene.2016.11.208.

[17] Cornelius W, Huellmantel LW, Mitchell HR. Ammonia as an engine fuel. SAE Tech Pap 1965;650052. doi:10.2307/44460524.

[18] Starkman ES, Newhall HK, Sutton R, Maguire T, Farbar L. Ammonia as a Spark Ignition Engine Fuel: Theory and Application. SAE Tech Pap 1966;660155. doi:10.4271/660155.

[19] Sawyer RF, Starkman ES, Muzio L, Schmidt WL. Oxides of Nitrogen in the Combustion Products of an Ammonia Fueled Reciprocating Engine. SAE Tech Pap 1968;680401. doi:10.4271/680401.

[20] Liu R, Ting DS-K, Checkel MD. Ammonia as a Fuel for SI Engine. SAE Tech Pap 2003.

[21] Grannell SM, Assanis DN, Bohac S V., Gillespie DE. The Fuel Mix Limits and Efficiency of a Stoichiometric, Ammonia, and Gasoline Dual Fueled Spark Ignition Engine. J Eng Gas Turbines Power 2008;130:042802: 1-8. doi:10.1115/1.2898837.

[22] Grannell SM, Assanis DN, Gillespie DE, Bohac S V. Exhaust Emissions From a Stoichiometric, Ammonia and Gasoline Dual Fueled Spark Ignition Engine. Proc. ASME Intern. Combust. Engine Div., Milwaukee, Wisconsin, USA: 2009, p. 135–41. doi:10.1115/ices2009-76131.

[23] Mørch CS, Bjerre A, Gøttrup MP, Sorenson SC, Schramm J. Ammonia/hydrogen mixtures in an SI-engine: Engine performance and analysis of a proposed fuel system. Fuel 2011;90:854–64. doi:10.1016/j.fuel.2010.09.042.

[24] Comotti M, Frigo S. Hydrogen generation system for ammonia-hydrogen fuelled internal combustion engines. Int J Hydrogen Energy 2015;40:10673–86. doi:10.1016/j.ijhydene.2015.06.080.

[25] Pozzana G, Bonfanti N, Frigo S, Doveri N, Dario P, Mattoli V, et al. A Hybrid Vehicle Powered by Hydrogen and Ammonia. SAE Tech Pap 2012. doi:10.4271/2012-32-0085.

[26] Frigo S, Gentili R, De Angelis F. Further insight into the possibility to fuel a SI engine with ammonia plus hydrogen. SAE Tech Pap 2014. doi:10.4271/2014-32-0082.

[27] Frigo S, Gentili R. Analysis of the behaviour of a 4-stroke Si engine fuelled with ammonia and hydrogen. Int J Hydrogen Energy 2013;38:1607–15. doi:10.1016/j.ijhydene.2012.10.114.

[28] Frigo S, Gentili R, Doveri N. Ammonia Plus Hydrogen as Fuel in a S.I. Engine: Experimental Results. SAE Tech Pap 2012. doi:10.4271/2012-32-0019.

[29] Koike M, Miyagawa H, Suzuoki T, Ogasawara K. Ammonia as a hydrogen energy carrier and its application to internal combustion engines. Woodhead Publishing Limited; 2012. doi:10.1533/9780857094575.

[30] Westlye FR, Ivarsson A, Schramm J. Experimental investigation of nitrogen based emissions from an

ammonia fueled SI-engine. Fuel 2013;111:239–47. doi:10.1016/j.fuel.2013.03.055.

[31] Ryu K, Zacharakis-Jutz GE, Kong SC. Effects of gaseous ammonia direct injection on performance characteristics of a spark-ignition engine. Appl Energy 2014;116:206–15. doi:10.1016/j.apenergy.2013.11.067.

[32] Ryu K, Zacharakis-Jutz GE, Kong SC. Performance enhancement of ammonia-fueled engine by using dissociation catalyst for hydrogen generation. Int J Hydrogen Energy 2014;39:2390–8. doi:10.1016/j.ijhydene.2013.11.098.

[33] Lhuillier C, Brequigny P, Contino F, Mounaïm-Rousselle C. Performance and Emissions of an Ammonia-Fueled SI Engine with Hydrogen Enrichment. SAE Tech Pap 2019.

[34] Lhuillier C, Brequigny P, Contino F, Mounaïm-Rousselle C. Combustion Characteristics of Ammonia in a Modern Spark-Ignition Engine. SAE Tech Pap 2019. doi:10.4271/2019-24-0237.

[35] Linstrom PJ, Mallard WG. NIST Chemistry WebBook, NIST Standard Reference Database Number 69,. 20899th ed. Gaithersburg MD: National Institute of Standards and Technology; n.d. doi:https://doi.org/10.18434/T4D303.

[36] Ryu K, Zacharakis-Jutz GE, Kong S-C. Effects of gaseous ammonia direct injection on performance characteristics of a spark-ignition engine. Appl Energy 2014;116:206–15. doi:10.1016/j.apenergy.2013.11.067.

[37] Zhou J, Richard S, Mounaïm-Rousselle C, Foucher F. Effects of Controlling Oxygen Concentration on the Performance, Emission and Combustion Characteristics in a Downsized SI Engine. SAE Tech Pap 2013. doi:https://doi.org/10.4271/2013-24-0056.

[38] Tazerout M, Le Corre O, Stouffs P. Compression Ratio and TDC calibrations using Temperature - Entropy Diagram. SAE Tech Pap 1999. doi:10.4271/1999-01-3509.

[39] Tazerout M, Le Corre O, Rousseau S. TDC Determination in IC Engines Based on the Thermodynamic Analysis of the Temperature-Entropy Diagram. SAE Tech Pap 1999;1999-01–14. doi:10.4271/1999-01-1489.

[40] Heywood JB. Internal Combustion Engine Fundamentals. McGraw-Hil. 1988. doi:10987654.

[41] Hohenberg G. Advanced approaches for heat transfer calculations. SAE Tech Pap 1979;790825.

[42] Goldmann A, Dinkelacker F. Approximation of laminar flame characteristics on premixed

ammonia/hydrogen/nitrogen/air mixtures at elevated temperatures and pressures. Fuel 2018;224:366–78. doi:10.1016/j.fuel.2018.03.030.

[43] Mathieu O, Petersen EL. Experimental and modeling study on the high-temperature oxidation of Ammonia and related NOx chemistry. Combust Flame 2015;162:554–70. doi:10.1016/j.combustflame.2014.08.022.